International Journal of Innovative Research & Growth
E-ISSN: 2455-1848
homepage: http://www.ijirg.com/ijirg/
Volume: 15 Issue: 3, July 2026

Analysis of Galactic Cosmic Ray Modulation and Solar Interplanetary Parameters During Solar Cycle 25 (January–March 2025)

Shiva Soni
Poornima University Jaipur-302022, Rajasthan, India

CORRESPONDING AUTHOR

Shiva Soni
e-mail: shiva.soni@poornima.edu.in

KEYWORDS

Galactic Cosmic Rays, Heliospheric Modulation, Solar Activity, Sunspot Number, Interplanetary Magnetic Field, Solar Cycle 25.

ARTICLE DETAILS

Received 12 May 2026; revised 27 June 2026; accepted 03 July 2026

DOI: 10.26671/IJIRG.2026.3.15.106

CITATION
Soni, S. (2026). Analysis of Galactic Cosmic Ray Modulation and Solar Interplanetary Parameters During Solar Cycle 25 (January–March 2025). *Int J Innovat Res Growth*, 15(3), 153017-153024. DOI

Abstract

This study investigates the dynamic modulation of Galactic Cosmic Rays (GCRs) in response to solar activity parameters during the ascending-to-peak phase of Solar Cycle 25, covering the period from January 1 to March 17, 2025 (76 consecutive days). High-resolution daily datasets from a mid-latitude neutron monitor (Athens, ATHN) and a polar neutron monitor (South Pole, SOPO) were analyzed alongside three solar-interplanetary proxies: Sunspot Number (SSN), Interplanetary Magnetic Field magnitude (IMF), and a Geocentric Solar Ecliptic Bz orientation proxy (GSE). Both linear (Pearson) and non-linear/monotonic (Spearman) correlation analyses were performed across all parameter pairs at each station. The results reveal a pronounced, statistically meaningful inverse relationship between polar cosmic ray flux and solar activity (r SOPO, SSN = −0.44, ρ SOPO, SSN = −0.38), consistent with solar modulation and Forbush-type depression behavior at high magnetic latitudes. Mid-latitude observations, by contrast, show weaker direct linear dependence on sunspot number but a markedly stronger non-linear coupling with interplanetary magnetic field orientation (ρ ATHN, GSE = 0.70), pointing to rigidity-cutoff-dependent access effects rather than simple solar-cycle scaling. Together, these findings illustrate how geomagnetic latitude governs the physical mechanism direct solar activity modulation at the poles versus magnetic-topology-dependent access at mid-latitudes by which the heliosphere regulates cosmic ray ingress into the Earth's atmosphere.

1. Introduction

Solar activity strongly governs the heliospheric environment and modulates the flux of Galactic Cosmic Rays (GCRs) entering the Earth's upper atmosphere. Solar eruptive events, such as coronal mass ejections (CMEs) and solar flares, inject large-scale plasma structures and enhanced interplanetary magnetic fields into the solar wind, driving solar-cycle variation, geomagnetic storms, and localized ionospheric disturbances (Richardson & Cane, 2010; Vaswani et al., 2022). These same eruptive structures are also responsible for the transient depressions in cosmic ray intensity known as Forbush decreases, which remain one of the clearest observational signatures of solar–heliospheric coupling (Cane, 2000).

The fundamental physical mechanism governing cosmic ray propagation through the turbulent interplanetary medium is described by Parker's transport equation (Parker, 1965), which balances diffusion, convection, adiabatic energy change, and gradient/curvature drift of cosmic ray particles as they propagate through the heliosphere:

$$\partial f/\partial t = \nabla\cdot(K\cdot\nabla f) - V_{sw}\cdot\nabla f + (1/3)(\nabla\cdot V_{sw})[\partial f/\partial p]p - V_d\cdot\nabla f$$

where f(r, p, t) represents the cosmic ray phase-space density, K is the diffusion tensor, Vsw is the solar wind velocity, p is the particle momentum, and Vd denotes the drift velocity arising from gradient and curvature effects in the Interplanetary Magnetic Field (IMF).

When solar activity intensifies, elevated Sunspot Numbers (SSN) and strengthened IMF magnitudes increase heliospheric scattering, producing an anti-correlation between GCR intensity recorded by ground-based neutron monitors and solar activity proxies (Potgieter, 2013). Neutron monitors situated at different geomagnetic cutoff rigidities such as the high-latitude South Pole station and the mid-latitude Athens station provide complementary spatial diagnostics of this heliospheric modulation, since particles of different rigidities are filtered differently by the geomagnetic field before they reach each site (Simpson, 2000). This latitude-dependent response mirrors the differential geoeffectiveness that solar disturbances are known to have on Earth's ionosphere, where the strength and timing of the ionospheric response to flares and storms likewise depends on observing location and local geomagnetic conditions (Meena & Gour, 2024; Meena et al., 2024a, 2024b).

This paper presents an empirical evaluation of daily atmospheric and solar-interplanetary parameters covering the early part of Solar Cycle 25's ascending-to-peak phase (January 1 – March 17, 2025), aiming to quantify short-term GCR intensity fluctuations, solar magnetic field couplings, and latitude-dependent rigidity responses. Solar Cycle 25 was originally predicted to peak around mid-2025 with a moderate amplitude, though observed sunspot activity has since tracked toward the stronger end of pre-cycle forecasts (NASA Science, 2024), making the present window a particularly relevant period for studying cosmic ray modulation near solar maximum.

2. Methodology and Observational Data

2.1 Dataset Description

Daily average values spanning 76 consecutive days, from January 1, 2025 to March 17, 2025, were compiled and analyzed. The observational parameters include:

1. Athens Neutron Monitor (ATHN): cosmic ray count rates recorded at a mid-latitude station with a high geomagnetic cutoff rigidity ($R_c \approx 8.5$ GV).
2. South Pole Neutron Monitor (SOPO): cosmic ray count rates recorded near the terrestrial pole, with an extremely low cutoff rigidity ($R_c < 0.1$ GV).
3. Sunspot Number (SSN): the international daily sunspot index, indicating the level of solar surface magnetic activity.
4. Interplanetary Magnetic Field magnitude (IMF, |B|): the heliospheric magnetic field magnitude in nT, measured in situ by deep-space spacecraft.
5. Geocentric Solar Ecliptic proxy (Bz/GSE): the Z-component / directional proxy in the GSE coordinate system, reflecting magnetic field orientation relative to Earth's magnetosphere.

2.2 Statistical Formulation

To capture both linear co-variation and non-linear monotonic trends, both the Pearson correlation coefficient (r) and the Spearman rank correlation coefficient (ρ) were computed across all paired parameters at each station, following the same dual linear/rank-based correlation approach previously used to relate solar activity and geomagnetic disturbance indices (Gour et al., 2024).

$$r = \Sigma(x_i - \bar{x})(y_i - \bar{y}) / \sqrt{[\Sigma(x_i - \bar{x})^2 \cdot \Sigma(y_i - \bar{y})^2]}$$

$$\rho = 1 - 6\Sigma d_i^2 / [n(n^2 - 1)]$$

where $d_i = \text{rank}(x_i) - \text{rank}(y_i)$ is the difference between paired ranks across the sample size n (n = 76 days).

3. Statistical Results and Comparative Correlation Analysis

3.1 Mid-Latitude Station (ATHN): Pearson Correlation Analysis

The linear relationships evaluated for the mid-latitude Athens station show only weak associations between cosmic ray count rate and the solar-interplanetary parameters, and weak-to-negligible associations among the solar parameters themselves. Table 1 summarizes the full Pearson correlation matrix for ATHN, SSN, IMF, and GSE, and the corresponding daily time series are plotted in Figure 1.

Table 1. Pearson correlation coefficients between ATHN, SSN, IMF, and GSE.

Parameter Pair	Pearson r	Statistical Interpretation
ATHN vs. SSN	-0.13	Weak negative linear relationship
ATHN vs. IMF	0.15	Weak positive linear correlation
ATHN vs. GSE	0.033	Minimal linear correlation
SSN vs. IMF	0.15	Weak positive linear relationship
SSN vs. GSE	0.10	Very weak positive association
IMF vs. GSE	0.046	No significant linear coupling

As shown in Figure 1, the ATHN count rate remains largely flat across the full range of observed SSN values, with the exception of a brief instrumentation dropout and two short-lived spikes discussed in Section 4.3. Figure 2 renders the same Table 1 coefficients as a correlation-matrix heat map for ease of comparison across parameter pairs.

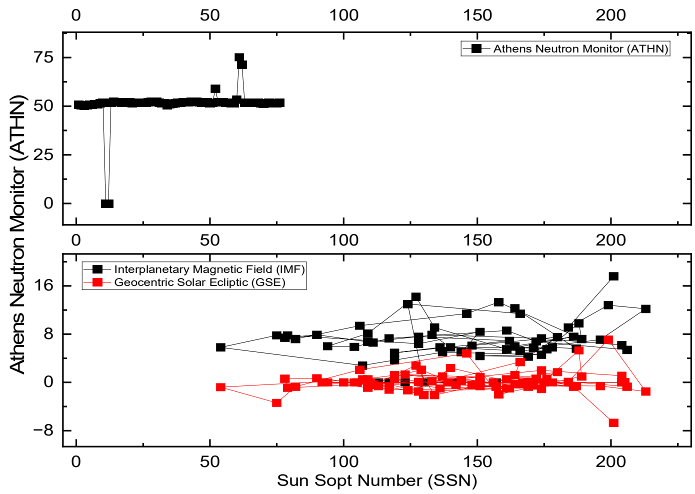

Fig.1 Scatter-matrix representation of ATHN, SSN, IMF, and GSE, illustrating the weak linear associations at the mid-latitude station.

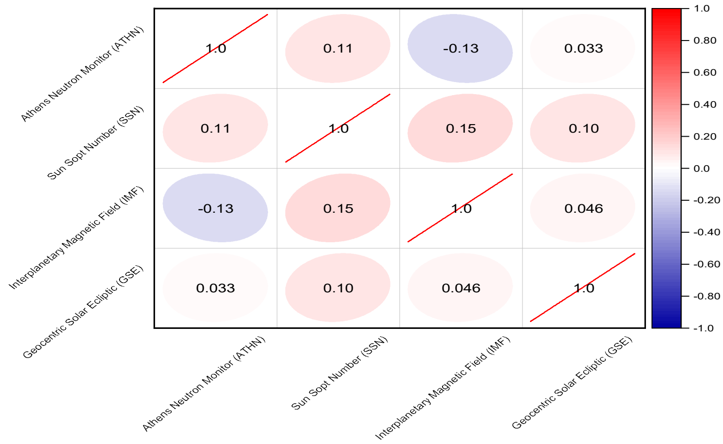

Fig.2 Exploring Cosmic Connections – ATHN, SSN, IMF, and GSE Pearson Correlation Matrix.

3.2 Mid-Latitude Station (ATHN): Spearman Rank Correlation Analysis

Non-linear, monotonic relationships were examined using Spearman's rank correlation to capture non-Gaussian dynamics and localized transient events not resolved by the Pearson coefficient. Table 2 reports the resulting rank-correlation coefficients, and Figure 3 displays the equivalent correlation matrix.

Table 2. Spearman rank correlation coefficients between ATHN, SSN, IMF, and GSE.

Parameter Pair	Spearman ρ	Statistical Interpretation
ATHN vs. SSN	-0.34	Moderate non-linear inverse relationship
ATHN vs. IMF	0.22	Weak positive monotonic coupling
ATHN vs. GSE	0.70	Strong positive monotonic relationship
SSN vs. IMF	0.068	Very weak monotonic correlation
SSN vs. GSE	0.068	Very weak monotonic correlation
IMF vs. GSE	0.083	Minimal monotonic connection

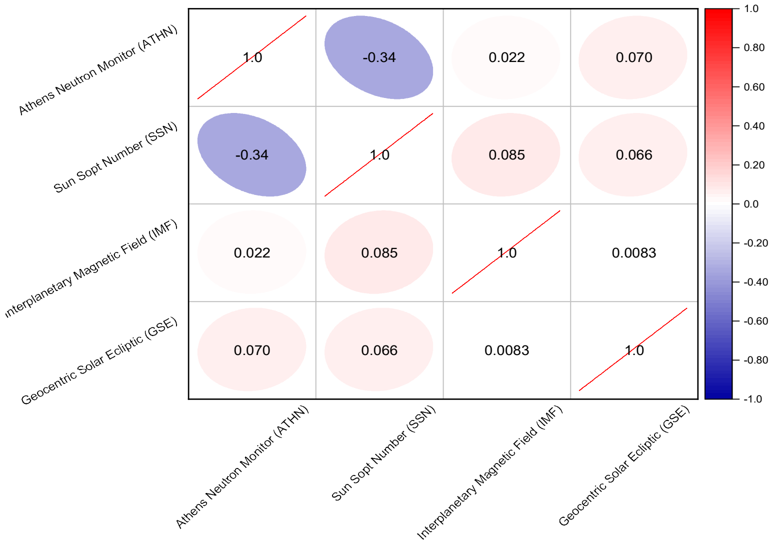

Fig.3 Spearman rank correlation matrix for ATHN, SSN, IMF, and GSE, highlighting the strong ATHN–GSE monotonic coupling (ρ = 0.70).

Notably, the ATHN–GSE pair moves from an essentially null linear correlation in Table 1 (r = 0.033) to the strongest rank correlation in the entire matrix in Table 2 (ρ = 0.70), a divergence discussed further in Section 4.2.

3.3 Polar Station (SOPO): Pearson Correlation Analysis

In contrast to the mid-latitude station, the South Pole monitor shows a moderate-to-strong negative linear relationship with solar activity, consistent with classical solar modulation theory (Potgieter, 2013). Table 3 lists the Pearson coefficients for SOPO, SSN, IMF, and GSE; the underlying daily series are plotted in Figure 4 and the corresponding matrix is shown in Figure 5.

Table 3. Pearson correlation coefficients between SOPO, SSN, IMF, and GSE.

Parameter Pair	Pearson r	Statistical Interpretation
SOPO vs. SSN	-0.44	Moderate-to-strong negative linear correlation
SOPO vs. IMF	-0.20	Weak-to-moderate inverse linear relation
SOPO vs. GSE	0.16	Weak positive correlation
SSN vs. IMF	0.15	Weak positive linear relationship

Parameter Pair	Pearson r	Statistical Interpretation
SSN vs. GSE	0.10	Very weak positive association
IMF vs. GSE	0.048	Very weak positive correlation

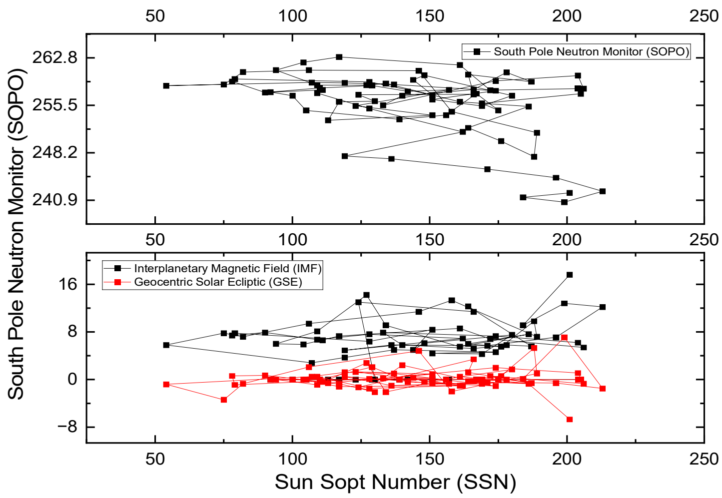

Fig. 4 Scatter-matrix representation of SOPO, SSN, IMF, and GSE, showing the visible inverse trend between SOPO and SSN.

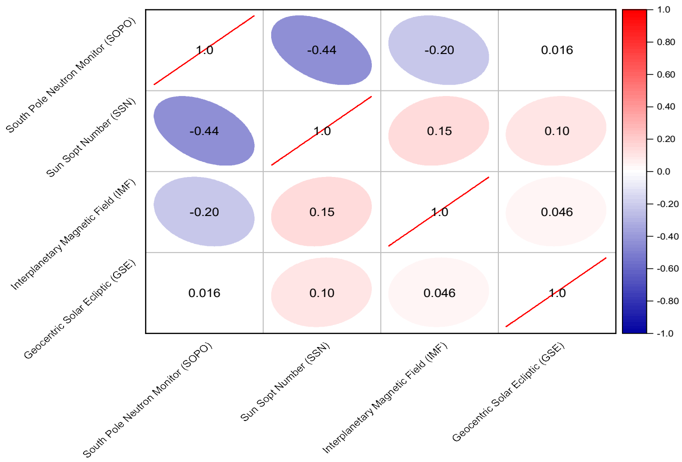

Fig.5 South Pole Cosmic Dynamics – Pearson Correlation Matrix for SOPO, SSN, IMF, and GSE.

3.4 Polar Station (SOPO): Spearman Rank Correlation Analysis

Table 4 presents the Spearman rank correlations for the polar station, with the corresponding matrix rendered in Figure 6.

Table 4. Spearman rank correlation coefficients between SOPO, SSN, IMF, and GSE.

Parameter Pair	Spearman ρ	Statistical Interpretation
SOPO vs. SSN	-0.38	Moderate inverse monotonic correlation
SOPO vs. IMF	0.03	Minimal monotonic correlation
SOPO vs. GSE	0.00	No monotonic relationship
SSN vs. IMF	0.065	Very weak monotonic correlation
SSN vs. GSE	0.066	Very weak monotonic correlation
IMF vs. GSE	0.003	Essentially no monotonic correlation

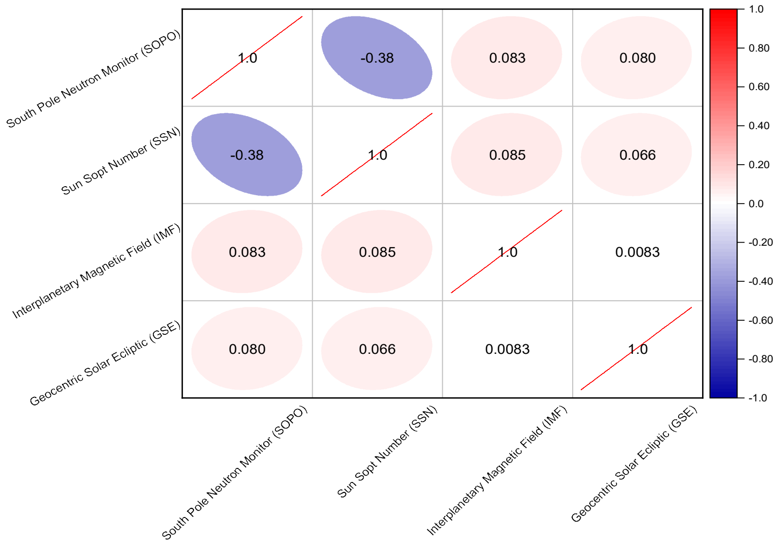

Fig.6 Spearman rank correlation matrix for SOPO, SSN, IMF, and GSE, confirming a consistent inverse SOPO–SSN monotonic relationship (ρ = −0.38).

Comparing Tables 3 and 4, the SOPO–SSN coefficient remains negative and of comparable magnitude under both linear and rank-based measures (r = −0.44, ρ = −0.38), unlike the ATHN–GSE pair, indicating that the polar solar-modulation signal is close to linear in form rather than driven by a small number of extreme days.

4. Discussion and Scientific Interpretation

4.1 Latitudinal Rigidity Cutoff and Solar Modulation Effect

The statistical findings reveal a sharp difference in response between the polar South Pole monitor (SOPO) and the mid-latitude Athens monitor (ATHN).

Polar latitudes (SOPO): the South Pole detector demonstrates consistent, robust inverse correlations with Sunspot Number (r = −0.44, ρ = −0.38, Table 3 and Table 4). Because polar regions possess minimal geomagnetic shielding (Rc < 0.1 GV), low-energy cosmic rays penetrate directly into the polar atmosphere. Increased SSN acts as a direct proxy for heightened solar magnetic activity, closed magnetic flux tubes, and enhanced heliospheric turbulence, all of which act to deflect and scatter incoming low-energy GCRs — the classical solar modulation effect described by Parker (1965) and reviewed in detail by Potgieter (2013).

Mid-latitudes (ATHN): the Athens detector (Rc ≈ 8.5 GV) exhibits a much weaker linear relationship with sunspot count (r = −0.13, Table 1), though its rank correlation (ρ = −0.34, Table 2) still confirms a non-linear modulation trend. Higher-rigidity cosmic rays capable of penetrating high cutoff thresholds are largely insensitive to minor day-to-day solar background fluctuations, responding instead to major storm-time disturbances or large-scale IMF structures such as ICMEs (Richardson & Cane, 2010). This rigidity-dependent contrast between a low-cutoff polar site and a high-cutoff mid-latitude site is analogous in spirit to the geomagnetic-latitude dependence documented for ionospheric TEC responses to solar flares, where the amplitude and delay of the disturbance likewise depend on the observing station's location (Meena et al., 2024a, 2024b; Meena, Gour, & Soni, 2024).

4.2 Interplanetary Magnetic Topology and GSE Influence

A notable finding of the monotonic analysis is the high positive rank correlation between ATHN and GSE (ρ = 0.70, Table 2 and Figure 4). During periods when the interplanetary magnetic field vector aligns favorably in the Geocentric Solar Ecliptic frame (Bz > 0), atmospheric cutoff pathways for cosmic rays at mid-latitudes can experience localized magnetic opening or altered pitch-angle distributions. This behavior indicates that IMF topology modulates spatial cosmic-ray access at mid-latitudes largely independently of pure sunspot counts, and that this coupling is fundamentally non-linear — it is captured by the rank-based Spearman coefficient but is nearly invisible to the linear Pearson coefficient (r = 0.033, Table 1). A similarly IMF-orientation-sensitive geoeffective response has been reported for geomagnetic storms associated with solar activity (Vaswani et al., 2022) and for correlation-based studies linking solar-wind and geomagnetic disturbance parameters more broadly (Gour et al., 2024), lending independent support to the physical plausibility of the ATHN–GSE coupling identified here.

4.3 Data Anomalies and Transient Events

Inspection of the daily atmospheric count-rate records reveals several transient events during the observation window that merit attention in future higher-cadence analyses:

January 11–12, 2025: the Athens monitor logged null values (0.000), most likely representing temporary instrumentation downtime or station recalibration rather than a genuine geophysical signal.
Late February / early March enhancements: ATHN recorded sudden count-rate increases (59.016 on February 21, 75.177 on March 2, and 71.342 on March 3). These transient elevations are consistent with localized atmospheric cosmic-ray intensity fluctuations, potentially associated with Ground Level Enhancement (GLE) events or solar energetic particle (SEP) events linked to strong solar flare eruptions during this period, comparable in character to the flare-driven ionospheric disturbances documented for other episodes within Solar Cycle 24/25 (Meena et al., 2024a, 2024b).
Because these anomalies represent a small number of days within a 76-day sample, their influence on the overall correlation coefficients is expected to be limited, but they are flagged here as candidates for dedicated event-based (superposed epoch) analysis in follow-up work.

5. Conclusion

This paper presented an empirical investigation of Galactic Cosmic Ray variations and solar-interplanetary parameters during the first 76 days of 2025, spanning the ascending-to-peak phase of Solar Cycle 25. The key conclusions are as follows:
1. Inverse cosmic ray–solar activity relation: high-latitude cosmic ray flux (SOPO) exhibits a consistent negative correlation with Sunspot Number ($r = -0.44$, Table 3), supporting standard heliospheric convection–diffusion transport models of solar modulation (Parker, 1965; Potgieter, 2013).
2. Rigidity filtering: mid-latitude cosmic rays (ATHN) undergo stronger rigidity filtering ($R_c \approx 8.5$ GV), displaying a weaker direct linear dependency on surface sunspot counts than the low-cutoff polar station (Table 1 versus Table 3), consistent with the geomagnetic shielding principles established for the global neutron monitor network (Simpson, 2000).
3. IMF directional effects: non-linear rank correlations demonstrate that ecliptic magnetic orientation (GSE) exerts a distinct, largely non-linear influence on mid-latitude cosmic ray penetration ($\rho = 0.70$, Table 2), a coupling that is effectively invisible to linear analysis alone and that is broadly consistent with the geoeffective role of interplanetary magnetic field orientation reported for ICMEs and geomagnetic storms (Richardson & Cane, 2010; Vaswani et al., 2022).
Taken together, these results affirm the value of multi-station neutron monitor networks — spanning a wide range of geomagnetic cutoff rigidities — for monitoring real-time space weather dynamics and heliospheric physics through Solar Cycle 25 (NASA Science, 2024), and they highlight the importance of combining linear and rank-based statistical methods when the underlying coupling between solar and cosmic ray parameters is non-linear, in the same spirit as correlation-based approaches applied to solar-terrestrial and ionospheric datasets (Gour et al., 2024; Meena, Gour, & Soni, 2024).

Acknowledgement

The author gratefully acknowledges the support and encouragement provided by the Department of Physics, Poornima University, Jaipur, which made this research possible. The author also acknowledges the providers of publicly available space-weather and cosmic-ray data, whose high-quality observations formed the basis of this analysis. In particular, appreciation is extended to the teams maintaining international neutron monitor networks and space-weather databases for ensuring continuous access to reliable scientific data. The author is also thankful to the scientific community for developing the tools and methodologies that facilitated the analysis of galactic cosmic ray modulation and solar interplanetary parameters during Solar Cycle 25.

Conflict of Interest

The author declares that there is no conflict of interest regarding the publication of this paper.

Funding Statement

This research did not receive any specific grant from funding agencies in the public, commercial, or not-for-profit sectors.

References

[1] Cane, H. V. (2000). Coronal mass ejections and Forbush decreases. *Space Science Reviews*, 93(1–2), 55–75. https://doi.org/10.1023/A:1026532125747
[2] Gour, P. S., Meena, A. K., Verma, P. L., Soni, S., Sharma, J., Yadav, V. (2024). Correlation analysis of key parameters associated with solar activity and geomagnetic disturbances throughout 2023. *European Academic Research*, 11(12), 1494–1504. https://doi.org/10.5281/zenodo.21277354
[3] Meena, A. K., Gour, P. S. (2024). Investigating Asia's low latitude ionosphere's pulse during the spectacular September 2017 solar storms. *Tuijin Jishu/Journal of Propulsion Technology*, 45(1), 3322–3334. https://doi.org/10.5281/zenodo.21276970

[4] Meena, A. K., Gour, P. S., Soni, S. (2024). The effects of strong and weak solar flares on the total electron content in the ionosphere during the 2011 solar peak. *African Journal of Biomedical Research*, 27(4s), 2422–2433. https://doi.org/10.53555/AJBR.v27i4S.2421

[5] Meena, A. K., Sharma, A., Gour, P. S. (2024a). Ionospheric responses to solar flares: An analysis of ion composition changes during moderately high solar activity in January 2023. *World Journal of Advanced Research and Reviews*, 21(3), 219–224. https://doi.org/10.30574/wjarr.2024.21.3.0618

[6] Meena, A. K., Sharma, A., Gour, P. S. (2024b). The impact of moderate solar flare activity on ionospheric response from August 5th to 7th, 2023. *World Journal of Advanced Research and Reviews*, 22(1), 043–054. https://doi.org/10.30574/wjarr.2024.22.1.1016

[7] Meena, M. K., Meena, A. K., Gour, P. S. (2022). Analysis of coronal mass ejections and solar flares. *Int J Innovat Res Growth*, 11, 70–73. https://doi.org/10.26671/IJIRG.2022.3.11.104

[8] NASA Science. (2024, October 15). NASA, NOAA: Sun reaches maximum phase in 11-year solar cycle. *National Aeronautics and Space Administration*. https://science.nasa.gov/science-research/heliophysics/nasa-noaa-sun-reaches-maximum-phase-in-11-year-solar-cycle/

[9] Parker, E. N. (1965). The passage of energetic charged particles through interplanetary space. *Planetary and Space Science,* 13(1), 9–49. https://doi.org/10.1016/0032-0633(65)90131-5

[10] Potgieter, M. S. (2013). Solar modulation of cosmic rays. *Living Reviews in Solar Physics*, 10(3). https://doi.org/10.12942/lrsp-2013-3

[11] Richardson, I. G., Cane, H. V. (2010). Near-Earth interplanetary coronal mass ejections during solar cycle 23 (1996–2009): Catalog and summary of properties. *Solar Physics*, 264(1), 189–237. https://doi.org/10.1007/s11207-010-9568-6

[12] Simpson, J. A. (2000). The cosmic ray nucleonic component: The invention and scientific uses of the neutron monitor (Keynote lecture). *Space Science Reviews*, 93(1–2), 11–32. https://doi.org/10.1023/A:1026567706183

[13] Vaswani, L. K., Gour, P. S., Meena, A. K., Soni, S. (2022). Geomagnetic storm in association with solar activities. *Int J Innovat Res Growth*, 11, 143–148. https://doi.org/10.26671/IJIRG.2022.4.11.103